atmosphere

MDPI

Article

Closing the N-Budget: How Simulated Groundwater-Borne Nitrate Supply Affects Plant Growth and Greenhouse Gas Emissions on Temperate Grassland

Ralf Liebermann [1,*], Lutz Breuer [1,2], Tobias Houska [1], Steffen Klatt [3], David Kraus [3], Edwin Haas [3], Christoph Müller [4,5] and Philipp Kraft [1]

1 Institute for Landscape Ecology and Resources Management, Research Centre for BioSystems, Land Use and Nutrition (iFZ), Justus Liebig University Giessen, Heinrich-Buff-Ring 26, 35392 Giessen, Germany; lutz.breuer@umwelt.uni-giessen.de (L.B.); tobias.houska@umwelt.uni-giessen.de (T.H.); philipp.kraft@umwelt.uni-giessen.de (P.K.)

2 Center for International Development and Environmental Research, Justus Liebig University Giessen, Senckenbergstraße 3, 35390 Giessen, Germany

3 Institute of Meteorology and Climate Research–Atmospheric Environmental Research (IMK-IFU), Karlsruhe Institute of Technology (KIT), Kreuzeckbahnstraße 19, 82467 Garmisch-Partenkirchen, Germany; steffen.klatt@kit.edu (S.K.); david.kraus@kit.edu (D.K.); edwin.haas@kit.edu (E.H.)

4 Institute for Plant Ecology, Research Centre for BioSystems, Land Use and Nutrition (iFZ), Justus Liebig University Giessen, Heinrich-Buff-Ring 26, 35392 Giessen, Germany; CMueller@uni-giessen.de or christoph.mueller@ucd.ie

5 School of Biology and Environmental Science and Earth Institute, University College Dublin, Belfield, Dublin 4, Ireland

* Correspondence: rliebermann@gmx.net; Tel.: +49-641-99-37398

Received: 7 June 2018; Accepted: 12 October 2018; Published: 17 October 2018

Abstract: European groundwater reservoirs are frequently subject to reactive nitrogen pollution (N_r) owing to the intensive use of nitrogen (N) fertilizer and animal manure in agriculture. Besides its risk on human health, groundwater N_r loading also affects the carbon (C) and N cycle of associated ecosystems. For a temperate grassland in Germany, the long-term (12 years) annual average exports of N_r in form of harvest exceeded N_r inputs via fertilization and deposition by more than 50 kgN ha^{-1}. We hypothesize that the resulting deficit in the N budget of the plant-soil system could be closed by N_r input via the groundwater. To test this hypothesis, the ecosystem model LandscapeDNDC was used to simulate the C and N cycle of the respective grassland under different model setups, i.e., with and without additional N_r inputs via groundwater transport. Simulated plant nitrate uptake compensated the measured N deficit for 2 of 3 plots and lead to substantial improvements regarding the match between simulated and observed plant biomass and CO_2 emission. This suggests that the C and N cycle of the investigated grassland were influenced by N_r inputs via groundwater transport. We also found that inputs of nitrate-rich groundwater increased the modelled nitrous oxide (N_2O) emissions, while soil water content was not affected.

Keywords: biogeochemical ecosystem model; sensitivity analysis; uncertainty assessment; soil moisture; biomass production

1. Introduction

Carbon dioxide (CO_2) and nitrous oxide (N_2O) are two potent greenhouse gases (GHGs) whose atmospheric concentrations are on the rise involving fundamental adaptations of global biogeochemical

cycles [1]. In 2011, average atmospheric concentrations of CO_2 and N_2O were approx. 391 ppm and 324 ppb, representing a relative increase of 40% and 20% compared to preindustrial times [2]. In addition to being radiatively active, N_2O is the single most important depleting substance of stratospheric ozone [3], constituting an additional threat for life on earth. Globally, agricultural soils are with about 60% the strongest contributors to total anthropogenic N_2O emissions [4].

While N_2O production has always been associated with nitrogen (N) turnover, e.g., nitrification and denitrification, [5] intensification of agriculture during recent decades has considerably increased soil N_2O production and emissions [1]. This is mainly attributable to profuse or improper N fertilizer application for crop yield improvements. A further consequence of the enhanced use of N fertilizer is that nitrate (NO_3^-) accumulates in the soil and subsequently leaches into groundwater bodies leading to groundwater pollution and eutrophication of nearby surface water bodies. Erisman et al. [6] reported that from 2000 to 2003 almost half of the European groundwater and surface water monitoring stations exceeded average NO_3^- concentrations of 25 mg NO_3^- L^{-1}. At groundwater fed riparian zones, the lateral inflow of N-rich water creates a high N availability and variable oxic states in the soil. They are then becoming potential hotspots for denitrification [7], where incomplete NO_3^- reduction leads to intense pulses of N_2O emissions.

With the incentive of optimizing plant N uptake and avoiding N losses through N_2O outgassing and NO_3^- leaching, several studies [8–14] assessed N turnover in the plant-soil system. Efforts to quantify N_2O emissions from grasslands have led to the application of model simulations [15,16] based on environmental variables that were known to affect soil N_2O production (e.g., soil moisture, soil temperature). Further development aimed to improve model predictions by establishing a closer connection between the cycles of N, carbon (C) and water within the model structure. Combining these cycles in both model development and analysis is still rarely achieved [17,18], while even then lateral influences of groundwater and N transport are most often neglected. Exceptions are, e.g., the hydro-ecological model RHESSys [19], or the coupled hydro-biogeochemical models of the DNDC model family (Wetland-DNDC and MIKE SHE [20], CMF and LandscapeDNDC [21,22]). A substantial advancement in modelling the coupled hydro-biogeochemical interaction on the field scale has recently been reported [23].

Comprehensive process-based models are needed for a holistic investigation and understanding of the relevant processes contributing to GHG emissions and N transport. However, the complexity of the involved processes leads to a large number of equations considered in these models to describe them. A plethora of process parameters is used to parameterize these equations, which are often not known and cannot be measured directly. Moreover, the large number of parameters and insufficient computing capacities usually prevent a comprehensive calibration of the complete parameter space.

Frequently, many of these parameters are not crucial for model performance [24]. They can be identified by sensitivity analyses [25,26] and neglected during the calibration process. Subsequent calibration may be performed by optimizing for a single parameter set or for a range of acceptable parameter sets. Choosing range calibration may be favored, if the implicit assumption of a perfect model design or the existence of a single "best" simulation needs to be avoided, so that parameter uncertainty is accounted for right from the beginning [27]. This approach can be implemented by the Generalized Likelihood Uncertainty Estimation (GLUE, [28]) which also allows calibrating for several important target values (multi-objective resp. multi-variable calibration). Such calibration provides the advantage that the models ability to simulate several target values can be accurately assessed without aggregating the simulation performances of each target value into one objective function.

For this study, we aimed to investigate the effect of the inclusion of groundwater transport of dissolved NO_3^- in a grassland ecosystem simulation. We utilized long-term data from temperate, groundwater influenced permanent grassland to calibrate the process-based ecosystem model LandscapeDNDC [29]. The model considers the C and N cycle of a vertically discretized soil profile and was further developed in this study to include groundwater influence on vadose zone processes on plot scale. Calibration targeted harvested biomass, soil moisture and emissions of CO_2 and N_2O.

A GLUE-like calibration technique was applied to assess model performance individually for each target value as well as collectively based on the number of accepted simulations.

2. Materials and Methods

2.1. Field Site

The investigated temperate, permanent grassland is part of the "Environmental Monitoring and Climate Impact Research Station Linden" near Giessen, Germany (50°32′ N, 8°41.3′ E, 172 m a.s.l.). Local climatic conditions are characterized by annual precipitation of 579 mm and average air temperature of 9.7 °C for the period 1995–2009. The grassland has been cultivated while the soil remained undisturbed for over 100 years and was not irrigated during the investigated period. The vegetation has been described as an Arrhenatheretum elatioris Br.-Bl. Filipendula ulmaria sub-community on a stagnofluvic gleysol on loamy-sandy sediments over clay [30]. The grassland research area was established in 1993/94, followed by a Free Air Carbon dioxide Enrichment (FACE) experiment in 1997 to investigate the effects of rising atmospheric CO_2 concentrations [31]. For this study, only data from plots with ambient CO_2 concentrations were used.

We used data from the three plots A1, A2 and A3 with different hydrological characterizations. According to their respective average groundwater levels (agl), the plots can be classified as dry (A1, agl = −1.00 m), moderately wet (A3, agl = −0.75 m) and wet (A2, agl = −0.65 m). Groundwater is generally shallow and highly variable in this area, rising close to the surface for several times during the year. A slight South-North slope (ca. 2%) indicates potential lateral inflow of groundwater from the upslope croplands. Groundwater levels were measured several times per week during the investigation period, while measurements of groundwater NO_3^- concentration have been started in March 2015. Relevant measurement data can be found at http://www.face2face.center.

2.2. Data Implementation

Model driving data include information regarding soil properties, weather, N deposition, field management and ambient atmospheric CO_2 concentrations. All relevant soil information is presented in Table A1. Weather data has been measured on a daily time resolution including global radiation, air temperature, relative humidity and precipitation. Soil properties include texture, bulk density, pH as well as organic C and N content [31,32]. A general soil water profile was derived from soil water retention characteristics that had been measured for several soil depths for different points of the field site, but independent of the plot locations. The remaining measurements encompass soil water content (SWC, at soil depth 0–15 cm), harvested plant biomass and GHG emissions. Harvested plant biomass is total aboveground biomass that was manually clipped at 4 cm height. Plant N content has been measured together with biomass. GHG emissions, i.e., N_2O emissions (since 1997) and CO_2 emissions (since 1998), were measured at dusk, a period which corresponds best to the daily average flux (personal communication). GHG measurements were performed with opaque static chambers placed on the grassland soil. Since this impedes photosynthetic activity and at least reduces plant growth, we consider the measured CO_2 emissions to be total ecosystem respiration minus growth respiration (which defines how simulated CO_2 emissions are calculated). N_2O emissions have been aggregated to monthly mean values due their variable times of measurement and highly variable emission rates.

All measured data that have been used for model simulations are implemented according to 4 different categories: model initialization, driver data, parameters and calibration data. Initialization uses data that determine the initial conditions of model variables at the beginning of the simulation. They include the initial values of organic C and N content of the soil. Driver data are determining boundary conditions (forcing) of the simulation. They include management events (cutting, fertilizer application), weather data, N deposition and groundwater levels (interpolated to daily time resolution). Parameters are fixed ecosystem properties including soil properties (except for organic C and N

content), plant C–N ratio as well as concentrations of atmospheric CO_2 and groundwater NO_3^- (both set to be constant on average values due to missing information of temporal variability during the simulation period). Calibration data are measured data against which simulation outcome is tested. They include harvested plant biomass, soil water content and emissions of CO_2 and N_2O.

The data were collected at the three grassland plots A1, A2 and A3, showing no relevant (concerning vegetation) or quantifiable (concerning soil properties) differences except for groundwater levels and soil hydraulic properties between the plots. Soil hydraulic properties (wilting point, field capacity, hydraulic conductivity) were estimated using water retention curves and used either as fixed parameters or as ranges for calibration (see Section 2.5).

2.3. N Balance

Balancing the measured N fluxes on the field sites resulted in a deficiency in the N budget, i.e., the balance of measured N input against N output (see Figure 1). Measured N input consists of fertilizer and atmospheric deposition. These inputs have been calculated to be considerably lower than the measured N outputs, i.e., N_2O emissions and N harvest. Average N balance has been calculated from these measured N fluxes for the period 1997–2009 (see Table 1). The resulting deficit may be further enlarged since N losses by leaching or other gaseous N emissions (NH_3, NO, N_2) have not been measured. N input by biological fixation of atmospheric N_2 was also not measured and therefore neglected. We assume N input by N_2-fixation to be small compared to the other N inputs since N fixing bacteria are usually associated to legumes which cover only about 2% at the field site [31]. Other N related processes—especially N turnover processes in the soil (mineralization, denitrification, etc.)—are not (directly) represented in the N balance because they do not constitute any additional N inputs or outputs. Thus, establishing a complete overview of all N fluxes is presently not possible for our field site, which is why we can only calculate a minimum for the N deficit. Soil N pools show no indication of change, as average organic N for the uppermost 7.5 cm increased only from 0.44% in 1998 to 0.45% in 2013. Thus, the minimum required N uptake from the groundwater has been calculated to be as large as the measured surplus of N output minus N input (N harvest + N_2O emissions − N fertilization − N deposition). We assume that most of this groundwater-borne N is NO_3^- and not in form of organic N compound, which can play an important role in agricultural systems [33].

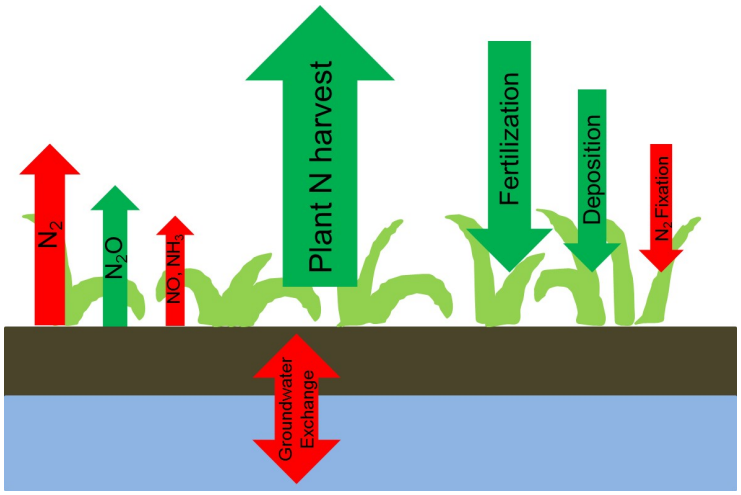

Figure 1. N fluxes of the investigated grassland. Green arrows correspond to measured quantities, red arrows represent unmeasured fluxes.

Table 1. Long-term average (1997–2009) and balance of measured N fluxes for the Linden FACE experiment.

Name	Average N Fluxes in kgN ha^{-1}		
	A1	**A2**	**A3**
Atmospheric N deposition	14	14	14
N fertilizer application	40	40	40
N_2O emission	−1	−1	−1
N removal by harvest	−106	−123	−129
N balance	−53	−70	−76

2.4. LandscapeDNDC: Model Setup

LandscapeDNDC [29] is an ecosystem model framework that provides an exchangeable pool of submodels for the description of various compartments (e.g., hydrology, vegetation and biogeochemistry) of forest [25,34,35], rainforests [36], grassland [17,37] as well as cropland ecosystems [38,39]. In this study the LandscapeDNDC submodel setup consists of four different submodels: grasslandDNDC (grDNDC, [39]) for plant physiology, soilchemistryDNDC (scDNDC, based on DNDC, [40]) for soil biogeochemistry, watercycleDNDC (wcDNDC, [41]) for hydrology as well as canopyECM [42] for microclimate. All submodels run consecutively with a daily time resolution. Generally, LandscapeDNDC considers an ecosystem to be homogenous in lateral direction. Vertically, the soil profile can be flexibly discretized. In this study, the vertical resolution was set to 50 mm for the upper soil layers, increasing to 150–200 mm for the lower layers. While the layers are different in respect of their respective soil properties, each layer is divided into several sublayers sharing the same characteristics. Sublayer thickness ranges from 10 mm for the upper layers to 50 mm for the lower layers. In order to test the influence of lateral groundwater flow and related transport of N (i.e., NO_3^-) on the overall N balance, the framework of LandscapeDNDC was technically enhanced by new simulation driving sources, i.e., daily information regarding groundwater table depth and mean nutrient concentration in the groundwater ($c_{x,g}$). The two submodels wcDNDC and scDNDC were adapted in order to account for the newly available information. For all soil layers z above the groundwater table z_g, wcDNDC calculates water flow v_w by the tipping bucket approach [41]. For all soil layers within the groundwater the water flow is set equal (1) to the last calculated water flow above the groundwater table v_w*:

$$v_w(z < z_g) = v_w^*, \quad (1)$$

The submodel scDNDC calculates the transport of all mobile N based on the simulated water flow of wcDNDC. N compounds that have passed the last soil layer are considered to be leached out of the simulation domain and no more available for further process calculations. For N compounds whose mean groundwater concentration is explicitly given as $c_{x,g}$, the adapted scDNDC calculates an additional N exchange rate τ_x (2) between the actual N concentration c_x after water flow transport and the mean N concentration in the groundwater $c_{x,g}$ by

$$\tau_x = K(c_{x,g} - c_x), \quad (2)$$

where K stands for a process parameter that determines the speed of the N exchange.

To trace the changes resulting from the contribution of groundwater in our model setup, all simulations have been run both with and without the groundwater module. Opposed to those simulations performed with no groundwater influence and no additional NO_3^- (noGW), the simulation with groundwater (withGW) provides plants and soil with an additional N source which is both specific to the plots and time dependent.

The simulation period started in April 1995 and ended in December 2009. The first two years were reserved for model spin-up, the calibration period started in 1997 (1998 for CO_2 emissions) and ended in 2009. Since the aim of the study is to investigate the explanatory and not the predictive capability of the model, no extra validation was necessary.

2.5. Sensitivity Analysis and Calibration

While field site properties, as they are represented in the model setup, can be fixed by using observations (see Section 2.2), uncertainty remains for the parameters determining processes in the modelled ecosystem. The plant physiology and the biogeochemical models comprise >100 uncertain process parameters (grDNDC: 12, scDNDC: 104) whose value can initially (i.e., before calibration) only be restricted to a predefined uncertainty range. In addition, the initialization of the model includes a variety of input parameters depending on the soil profile discretization. All soil input parameter values are derived from literature except for soil hydraulic properties, i.e., hydraulic conductivity, field capacity and wilting point, which have been measured. However, these bear some uncertainty, as they are difficult to quantify. The large number of process and input parameters prevents global calibration of all parameters due to insufficient computational capacities. Therefore, calibration was performed for the most sensitive parameters (see Table A2) only, which had been determined before via separate sensitivity analyses for each model setup. Uncertainty ranges for process parameters were provided beforehand. Uncertainty ranges for soil hydraulic properties have been estimated for the uppermost and lowermost soil layers by water retention curves [32] and expert knowledge about the field site. Values for intermediate soil layers were derived by interpolation.

In the following, all objective functions for sensitivity analysis and calibration are based on Root Mean Squared Error (RMSE). We calculated RMSE for each target value (N_2O, CO_2, biomass and SWC) as well as for each field site plots (A1, A2, A3), resulting in 12 objective functions. The free open source software SPOTPY (Statistical Parameter Optimization Tool for Python [43]) was used for all sensitivity analyses and calibration runs.

2.5.1. Sensitivity Analysis

Sensitivity analyses were based on 122 unknown parameters consisting of 6 soil hydraulic input parameters, 12 process parameters belonging to grDNDC and 104 to the scDNDC module (including one parameter belonging to the groundwater module, regulating the groundwater NO_3^- access rate). The Fourier Amplitude Sensitivity Test (FAST, see [44,45]) was used for all sensitivity analyses. FAST is a variance based sensitivity analysis, providing reliable sensitivity estimates also for nonlinear models and is therefore suited for our complex biogeochemical model. The final set of sensitive parameters for subsequent calibration was derived by individual sensitivity analyses for the two different model setups regarding groundwater (noGW and withGW). By assessing the parameter sensitivities with FAST, we combined our 12 objective functions to come up with not more than 25 parameters to be considered most sensitive (see Figure A1). For the withGW sensitivity analysis, we used groundwater levels from the moderately wet plot A3 and applied the selected sensitive parameters for calibration of A1, A2 and A3.

2.5.2. Calibration

All sensitive parameters were calibrated based on Latin Hypercube sampling [46]. For each calibration, the chosen LHS interval resolution resulted in four populations P_i (i = noGW, A1, A2, A3) with 600,000 parameter sets each. All P_i were individually evaluated (RMSE) with respect to the target values SWC, plant biomass, N_2O and CO_2 emissions. In order to quantify parameter-induced model uncertainty, a method similar to the Generalized Likelihood Uncertainty Estimation (GLUE, see [28,47,48]) was applied. In conformity with GLUE, we define the 25th percentile best performing parameter sets (and their corresponding simulations) as behavioural. According to four target values j = SWC, Biom, N_2O, CO_2, this creates four subpopulations of behavioral parameter sets with each population P_i: $P_{i,SWC}$, $P_{i,Biom}$, $P_{i,N2O}$, $P_{i,CO2}$. Subsequently, a set $P_{G,i}$ of global behavioral parameter sets for each population P_i was derived as the full intersection (see Figure 2) of all subpopulations $P_{i,j}$. While it is theoretically not guaranteed that the number of elements—which we will call intersection size—of each $P_{G,i}$ is non-zero, we avoided this problem through the choice of the threshold for behaviural

parameter sets. Pair-wise partial intersections, which are intersections of two $P_{i,j}$, have also been investigated, so that each target value can be analyzed according to its intersection with each of the other target values.

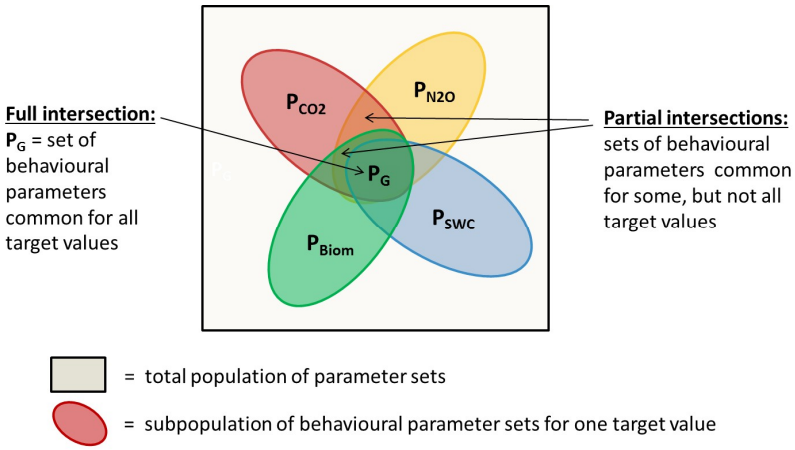

Figure 2. Multi-variable parameter calibration represented by intersections of behavioral parameter sets. The number of behavioral parameters common to several target values can give indication of model coherency.

The intersection sizes provide an indication of the models ability to simulate several target values at the same time. This ability, which we will call model coherency from now on, is quantifiable through the intersection sizes and shows how well the different subsystems are integrated within the model. This is most relevant since calibration of a single target value may diminish the performance of other target values. Therefore, the behavioral simulations for one target value may be entirely different to that of another target value, so that an intersection may be small or non-existent. The intersection sizes of the model setups noGW and withGW were compared to assess how the inclusion of the groundwater affects the model coherency. Additionally, intersection sizes are compared to a theoretical reference value that is derived from a hypothetical model that simulates four independent target values with the same threshold and the same number of iterations. Based on a population of 600,000 parameter sets and four independent subpopulations containing one quarter of these parameter sets, the expected number of behavioral simulations is $600{,}000 \times 0.25^4 = 2343.75$ (rounded to 2344).

For the noGW model setup, the three plots A1, A2, and A3 were considered to be indistinguishable, since in this case the only difference between the plots is given by their hydraulic properties, which are either calibrated or, in case of low sensitivity, approximated as equal among the plots. This means that for noGW, the behavioral parameter sets for the three plots have been drawn from the same population P_{noGW}. In contrast, for the model setup withGW, each plot was calibrated by its individual LHS-populations (P_{A1}, P_{A2}, P_{A3}).

3. Results

We begin with identification of the most sensitive parameters for each model setup and the intersection sizes for each model setup and plot. The intersection sizes show the number of simulations that form the basis of the plot-dependent uncertainty ranges of the annual NO_3^- uptake and the four target values in the following sections. These uncertainty ranges were aggregated into confidence intervals with a confidence coefficient of 95%.

3.1. Sensitive Parameters and Intersection Sizes

Out of the 122 unknown parameters, we identified 23 parameters to be the most sensitive for the noGW model setup and 21 parameters to be the most sensitive for withGW (14 parameters were most sensitive for both model setups (see Table A2).

The intersection sizes of full intersections, i.e., the number of parameter sets that are globally behavioural, varied between 50 and 500 (see Table 2), which is considerably lower than the reference value of 2344. The intersection sizes were slightly lower for withGW than for noGW. They strongly varied among the plots A1, A2 and A3: the largest intersections were found for A1, the lowest for A2. Sizes of the pair-wise partial intersections (see Table A5) showed the highest size of about 53,000 parameter sets for the intersection between P_{Biom} and P_{N2O}. P_{Biom} and P_{CO2} showed the lowest pair-wise partial intersection size of approximately 8200 parameter sets which is about 3 to 7 times smaller than any other pair-wise intersections.

Table 2. Intersection sizes: The number of global behavioural runs calculated for the plots A1, A2 and A3 and the model setups with and without groundwater influence (withGW and noGW). The reference value represents the expected value derived from a hypothetical model which simulates 4 uncoupled target values.

Model Setups	A1	A2	A3
noGW	471	73	427
withGW	469	58	395
reference value		2344	

3.2. NO_3^- Uptake

The minimum required N uptake or N deficit (see Section 2.3) has been calculated from measurements to be 53 kgN ha^{-1}, 70 N kg ha^{-1} and 76 kgN ha^{-1} for the plots A1, A2 and A3, respectively, averaged over the period from 1997–2009 (atmospheric N fixation, N leaching and non-N_2O emissions not included, see Table 1). For withGW simulations, annual NO_3^- uptake from groundwater show strong variations between the plots (Figure 3). Maximum NO_3^- uptake (i.e., the upper limit of the confidence intervals in Figure 3) is about twice as much for A2 (wet) than for A1 (dry). Simulated NO_3^- uptake for A1 is lower than the minimum required NO_3^- uptake to compensate the N deficit most of the time (green line close to or above the upper end of the blue area). NO_3^- uptake for A2 and A3 shows similar underestimation in the second half of the simulation period (2003–2004 for A2, 2003–2006 for A3), but is generally higher and within the confidence intervals for these wetter plots.

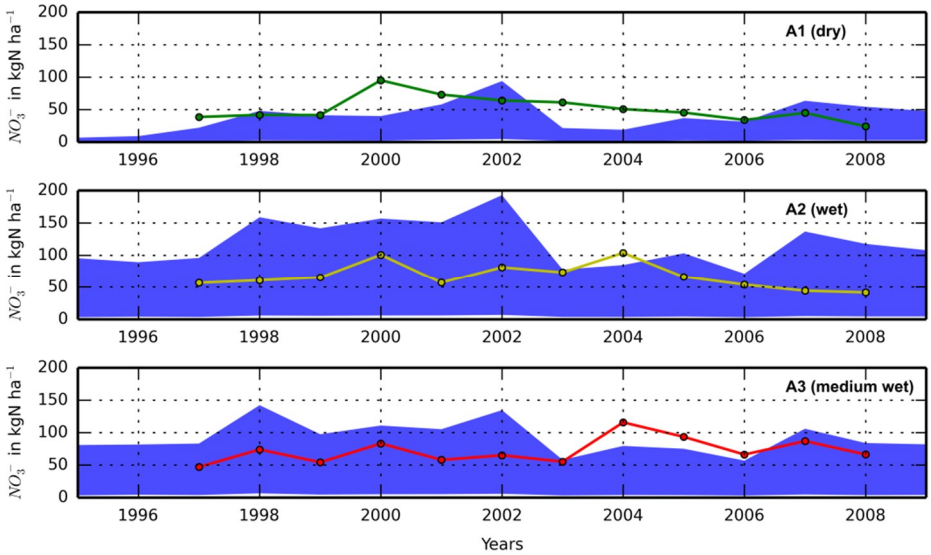

Figure 3. Confidence intervals (blue area) for the simulated annual NO_3^- uptake from groundwater for the plots A1, A2 and A3 (from top). Colored solid lines depict the minimum required NO_3^- uptake, which is necessary to close the deficit in the measured N budget. Additional information can be found in Tables A3 and A4.

3.3. Biomass

The biomass simulations (Figure 4) without groundwater (noGW) considerably underestimated the measured biomass harvest. The respective confidence intervals were lower than nearly all of the measurements. In contrast, for simulations with groundwater (withGW) most of the measured data points lie within the confidence intervals. The confidence intervals are larger for A2 (wet) and A3 (moderately wet) than for A1 (dry) which often tended to underestimate observations, especially at spring harvest. This is reflected RMSE values (Table 3) which are lower in withGW compared to noGW, with biomass simulations showing most improvement in the wetter plots A2 and A3. Measured spring harvests tend to be higher than summer harvests except for 2007. Here, measured spring harvest is lower than the summer harvest, whereby spring harvests is underestimated by the respective confidence intervals of A2 and A3, but not A1.

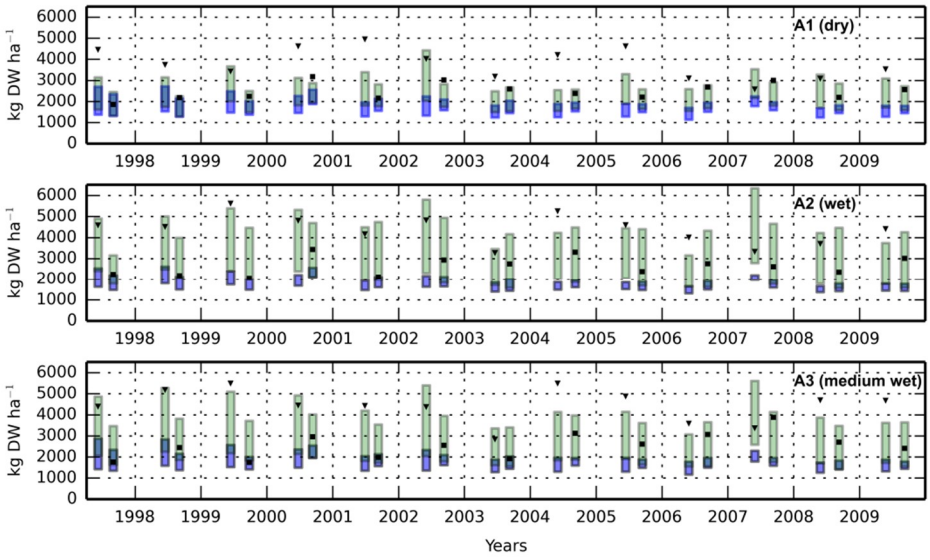

Figure 4. Measured data and simulated confidence intervals for the harvested biomass for the plots A1, A2 and A3 (from top). Confidence intervals for noGW simulations are shaded in light blue, withGW simulations are in light green and overlap between noGW and withGW in darker blue-green. Black triangles depict the spring harvests, black squares depict the late summer harvests. Additional information can be found in Tables A3 and A4.

Table 3. RMSE for behavioural simulation runs of harvested biomass.

Target Value	Plot	Minimum RMSE		Mean RMSE		Maximum RMSE		Measurements (Mean)
		noGW	withGW	noGW	withGW	noGW	withGW	
Biomass [kg ha^{-1}]	**A1**	1308	660	1572	1081	1952	1780	3040
	A2	1822	810	2002	1233	2226	1830	3585
	A3	1815	796	2088	1294	2434	2069	3348

3.4. N_2O Emissions

Measured N_2O emissions were mostly within the confidence intervals of both noGW and withGW (Figure 5), with the exception of multiple emission peaks. This is especially true for A1 where noGW and withGW confidence intervals are nearly identical but miss a series of emission peaks during 1998 to 1999. For A2, withGW confidence interval shows a higher upper limit than noGW that covers many of the peak emissions that are underestimated by noGW simulations (e.g., for the winter season of 2003/2004). Higher N_2O emissions at withGW simulations increased overestimation compared to noGW simulations, so that maximum RMSE values (Table 4) increased strongly at the wetter plots A2 and A3 for withGW simulations. In contrast, mean and minimum RMSE are mostly similar between noGW and withGW.

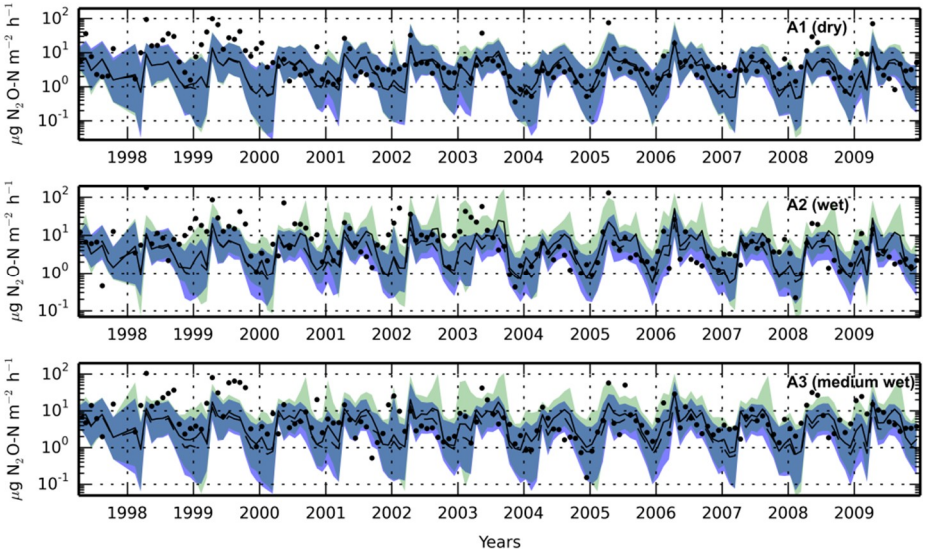

Figure 5. Measured data (black circles) and simulated confidence intervals for the monthly averaged N_2O emissions (calculated as N_2O-N) for the plots A1, A2 and A3 (from top). Confidence intervals for noGW simulations are shaded in light blue, withGW simulations are in light green and overlap between noGW and withGW in darker blue-green. Black lines depict the median for withGW (solid line) and noGW (dashed line) simulations. Additional information can be found in Tables A3 and A4.

Table 4. RMSE for behavioural simulation runs of N_2O emission.

Target Value	Plot	Minimum RMSE		Mean RMSE		Maximum RMSE		Measurements (Mean)
		noGW	withGW	noGW	withGW	noGW	withGW	
N_2O emissions [µgN m^{-2} h^{-1}]	**A1**	13.47	13.55	15.76	15.78	18.21	18.20	9.33
	A2	19.86	19.43	21.33	22.90	22.60	38.35	11.16
	A3	14.13	14.31	16.03	17.10	17.58	50.38	10.20

3.5. CO_2 Emissions

Observed CO_2 emissions were underestimated by the simulations, for noGW more so than for withGW. This is corroborated by minimum and mean RMSE values (Table 5) which are lower for withGW simulations than for noGW (even though maximum RMSE are slightly higher for withGW).

Table 5. RMSE for behavioural simulation runs of CO_2 emission.

Target Value	Plot	Minimum RMSE		Mean RMSE		Maximum RMSE		Measurements (Mean)
		noGW	withGW	noGW	withGW	noGW	withGW	
CO_2 emissions [mg m^{-2} h^{-1}]	**A1**	264.6	214.5	318.0	296.5	353.5	356.5	382.2
	A2	291.7	201.8	327.5	265.4	362.1	380.5	398.2
	A3	241.6	176.4	288.3	252.3	325.2	337.0	363.9

The mismatch between observations and simulations is particularly pronounced during summer periods where CO_2 emissions reach their maxima (Figure 6). The only exception is the dry summer season of 2003 where measured CO_2 emissions were low and withGW confidence intervals simulations where relatively high for the wetter plots A2 and A3. For winter seasons, agreement is considerably better for both noGW and withGW. Overall, withGW simulations clearly reduced minimum and mean RMSE while maxima of RMSE slightly increased (Table 5).

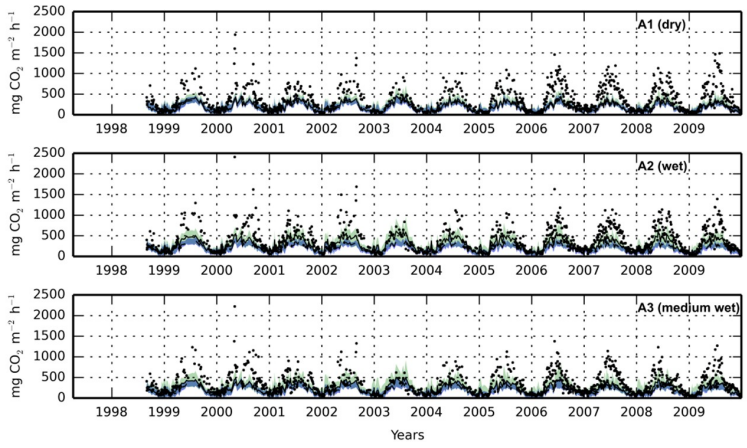

Figure 6. Measured data (black dots) and simulated confidence intervals for the CO_2 emissions for the plots A1, A2 and A3 (from top). Confidence intervals for noGW simulations are shaded in light blue, withGW simulations are in light green and overlap between noGW and withGW in darker blue-green. Black lines depict the median for withGW (solid line) and noGW (dashed line) simulations. Additional information can be found in Tables A3 and A4.

3.6. Soil Water Content

Match between SWC simulations and observations is small due to their very dissimilar overall variability, which is much higher for the observations (varying between 10 and 65% SWC, either relatively dry or moist for most data points) than for simulations (almost all values between 30 and 50% SWC). Soil water content (SWC) simulations are nearly identical between noGW and withGW, as can be seen in Figure 7. The dry spell in summer 2003, for example, is indicated by somewhat longer conditions of especially low measured SWC, but found no similar reaction in the simulations. Neither are the generally strong seasonal dynamics of SWC matched by any of the simulations for A1, A2 and A3. While for A1 (dry plot) the upper bounds of observations were captured reasonably well, this was less clear for A3 (medium wet) and not apparent for A2 (wet) at all. All model runs had particularly difficulties to simulate low SWC, specifically for A2 where the confidence interval for simulations was very small. Consequently all RMSE are nearly identical when comparing noGW and withGW simulations (Table 6).

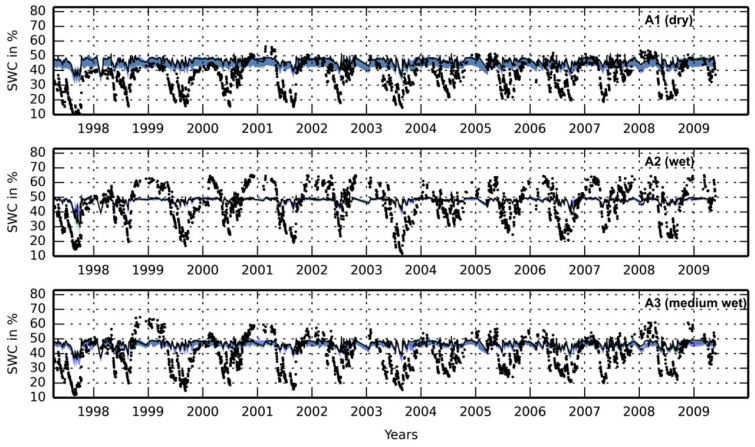

Figure 7. Measured data (black dots) and simulated confidence intervals for the soil water content at 0–15 cm for the plots A1, A2 and A3 (from top). Confidence intervals for noGW simulations are shaded in light blue, withGW simulations are in light green and overlap between noGW and withGW in darker blue-green. Black lines depict the median for withGW (solid line) and noGW (dashed line) simulations. Additional information can be found in Tables A3 and A4.

Table 6. RMSE for behavioural simulation runs of SWC.

Target Value	Plot	Minimum RMSE		Mean RMSE		Maximum RMSE		Measurements (Means)
		noGW	withGW	noGW	withGW	noGW	withGW	
SWC [%]	A1	9.66	10.05	13.42	13.46	14.67	14.80	34.86
	A2	11.28	11.54	12.07	12.01	12.73	12.59	43.62
	A3	10.75	11.39	12.82	13.18	13.75	14.00	37.55

4. Discussion

4.1. N Balance and Groundwater NO_3^-

The long-term N balance of the observed temperate grassland showed that N output, mainly harvest, exceeded N input by atmospheric deposition and fertilizer application by more than 50 kgN ha^{-1} per year (see Table 1). This deficit cannot be explained by measurement uncertainties or mineralization of organic N from the soil. It might be even larger, as several fluxes, like N_2 and NO emissions as well as NO_3^- leaching, are not included in the balance. Consequently, biomass calculated by LandscapeDNDC showed a severe underestimation of the observations (see Figure 4) if only measured N inputs are taken into account (noGW).

N budgets on ecosystem level are rarely investigated [49–51], especially in connection with deficits of this magnitude. Paustian et al. [52] found already in 1990 a surplus of N in harvest biomass and attributed it to an enhanced mineralization of the soil N storage due to plant roots. However, our findings are based on a long-term experiment that showed no change in the soil N storage over the course of 15 years (see Section 2.3), while the N deficit resulting from the balance calculated in Table 1 would have resulted in a depletion of soil N of at least 700 kg ha^{-1} in the period of 1997–2009 (53 kg ha^{-1} $year^{-1}$ × 13 years = 689 kg ha^{-1}). This goes in line with the noGW simulations that showed limited biomass production due to the N deficit, which increases with the gradual depletion of the soil N storage. LandscapeDNDC calculates the mineralization of the soil storage via bulk soil organic matter decomposition based on soil N content, SWC, soil temperature and acidity that does not differentiate between root, microbial and animal induced mineralization.

A different explanation for an N deficit is given by Watson et al. [53], who found that soil N accumulation in a grazed grassland exceeded N input and suggested N redistribution by upward water movement as a possible cause. For our study, the N deficit and periodically high groundwater levels drew attention to the influence of groundwater with the dissolved NO_3^- on the grassland ecosystem. N fertilizer application at adjacent croplands is a likely source for the long-term NO_3^- supply through shallow groundwater. Piezometer observations of soil water NO_3^- concentrations, which have recently (March 2015) been started as a consequence of the simulations, showed highest NO_3^- concentrations several weeks before fertilizer was applied at the grassland site. Furthermore, observations showed that the N deficit was less pronounced for the dry plot A1 (53 kg ha^{-1}, lowest groundwater levels) than for two wetter plots (A2: 70 kg ha^{-1}, A3: 76 kg ha^{-1}). Thus, lower groundwater levels at A1 are lowering the N deficit by either increasing drought stress due to reduced water availability or by reducing the NO_3^- supply from the groundwater. We assume the latter possibility to be more likely because groundwater levels are generally shallow at all plots, thus preventing extended drought periods. Though there are no studies to date linking the overall N budget to the groundwater at this site, previous investigations in our study area showed that most of the N_2O emissions can be traced back to denitrification processes in the soil layers below 20 cm [54], and are related to the groundwater level and soil depth [55].

4.2. Impact of Groundwater-Borne NO_3^- on Simulated Ecosystem Behaviour

LandscapeDNDC simulations focussed on harvested biomass, N_2O and CO_2 emissions as well as SWC because these target values are dependent on groundwater level and/or groundwater NO_3^- concentration. Integration of a simple groundwater module in LandscapeDNDC improved simulated

versus observed biomass production and CO_2 emissions by reducing the RMSE (see Tables 3 and 5). Biomass simulations severely underestimated observations at the noGW setup and could be evened out for plots A2 and A3 at withGW (Figure 4). Similar to biomass, simulated CO_2 emissions increased as a result of introducing groundwater NO_3^- (Figure 6), even though a (smaller) deficit due to underestimation of measured CO_2 emissions remained. This deficit of CO_2 emissions is largest for A1, so N limitation for this plot is still likely. Luo et al. [56] found that N fertilization can increase grassland CO_2 emissions due to enhanced soil respiration and reasoned that NO_3^- addition might have mitigated the N limitation of root biomass and soil microbial biomass. In contrast to CO_2 emissions, RMSE of simulated N_2O emissions (Table 4) did not improve due to groundwater N supply, even though N_2O emissions have also increased (Figure 5). The reason for this may be that N_2O production and release is highly dynamic, if not erratic, and rather related to 'hot moments' [7] like fertilizer application [8] and rainfall events [57] than on long-term N availability. Observed emission peaks are more frequent within the withGW confidence intervals than for noGW (Figure 5), which makes correct capture of sudden N_2O emission pulses more likely if groundwater NO_3^- is incorporated. Nevertheless, this has not led to an overall better agreement with measured N_2O emissions because we also calculated much higher maximum RMSE for withGW simulations at the 'wetter' plots A2 and A3.

Generally, the minimum required N input could be simulated well for the plots A2 and A3 by groundwater supply (Figure 3) in this study. Lower groundwater levels at plot A1 (see Section 2.1) likely reduced the N uptake from groundwater and impeded a complete balancing of the measured N deficit, even though the deficit was lower for A1 than for A2 and A3 (see Table 1). Reasons might be that LandscapeDNDC had to draw on average NO_3^- concentrations for calculating N uptake from groundwater or because other pathways of N input like atmospheric N_2 fixation or organic N supply via the groundwater have been mostly neglected in the model setups. Another issue is the large uncertainty of NO_3^- uptake, so that, even for plots A2 and A3, several behavioural simulations showed a low NO_3^- uptake from groundwater and did not even come close to balance the N deficit.

4.3. Groundwater, SWC and N_2O Emissions

LandscapeDNDC simulated SWC nearly identical for the model setups noGW and withGW (Figure 7), indicating that incorporating groundwater had no relevant effect on the simulated water balance. However, this cannot be proven since we did not investigate the partitioning of soil moisture due to precipitation versus groundwater. Given that the water balance remained largely unchanged, most differences between the simulations of noGW and withGW can be attributed to the function of groundwater as a transport medium for dissolved NO_3^-. Since SWC measurements show considerable differences between the plots, likely the consequence of different groundwater levels, this explains why our SWC simulations lack the high variability that can be found in the measurements. Similar problems were shown by Kröbel et al. [58] who applied watercycleDNDC to a floodplain in North China. Especially periods of high soil moisture are not well simulated by watercycleDNDC at our field site. Such periods occur due to water logging which is linked to the presence of pseudogley in the field soil. Up to a certain point, periods of water logging can be beneficial for NO_3^- uptake if high soil moisture alleviates plant drought stress during hot and dry summer periods. Nevertheless, we don't assume a strong connection between high soil moisture and NO_3^- uptake at our field site as it normally doesn't experience extended drought periods. Concerning the simulations, the simplicity of the applied tipping bucking approach might contribute to the overall lack of representation of high soil moisture periods as it is largely insensitive to capillary rise induced by high groundwater tables (the tipping bucket approach describes a simple infiltration routine, allowing the water to flow from one soil-layer into the other, if the capacity limit was reached).

The simulated soil hydrology is also an important factor of both simulated N_2O and CO_2 emissions through NO_3^- transport and SWC variability. Periods of high soil moisture, for example, affect the share of anaerobic microsites in the soil, resulting in an increase of N_2O production by denitrification [13]. Therefore, SWC and N_2O emissions are often simulated in combination such as in

the study by Saggar et al. [37] who applied NZ-DNDC (i.e., a version of DNDC tailored for applications in New Zealand) on grazed grassland. Similar to our results, they faced problems with capturing events of peak N_2O emissions even though they achieved better agreement of simulations with highly variable SWC measurements than we did. To date, only few simulation studies [20,22,23,59] addressed the issue of establishing a comprehensive connection between the cycles of water and N, and even less are able to show the effect of changing groundwater levels on N_2O emissions while including groundwater-borne N supply. For our grassland site, it is probable that measurements (and consequently also simulations) of N_2O emissions and SWC share only a weak connection. This is because we had to utilize SWC measurements from the uppermost 15 cm of soil, while most of the N_2O emissions originate from the deeper soil layers (see Section 4.1) where the impact of groundwater on SWC and N_2O production is especially strong.

4.4. CO_2 Emissions and SWC

Simulated and measured CO_2 emissions (Figure 6) showed a good correlation concerning the timing of the seasonal cycling. Moreover, we found a good match for the dry summer of 2003, even though simulated CO_2 emissions underestimated observations during the remaining summer seasons of the investigation period. Therefore, it seems reasonable for the plots A2 and A3 that insufficient SWC simulations (Figure 7) of high SWC impede our CO_2 emission simulations during the vegetation period. Xiang et al. [60], for example, showed that frequent cycles of drying and rewetting increase respiration in grassland soil and assumed that the increase is amplified for undisturbed deeper soil layers. Such respiration pulses due to rewetting are in line with our observed CO_2 emissions peaks during summer, and may be better simulated if simulated SWC is improved. Sándor et al. [61] performed multi-variable simulations of grasslands, and argued that problems with SWC simulations are partly responsible for insufficient results when simulating the C cycle. Zhang et al. [62] also modelled effects of soil moisture on simulated soil C turnover and tended to underestimate soil respiration pulses in summer, but this was alleviated by incorporation of additional soil C pools. This provides an example that the reasons for an underestimation of CO_2 emissions may be not because of simulation of SWC and NO_3^- supply alone, but also due to the way the C cycle is implemented in the model structure. Respiration because of photosynthetic activity was entirely excluded from our CO_2 emission simulation since measurements were performed with dark chambers. This may have led to underestimation in the simulation since it remains elusive how many growth-related processes requiring respiration are affected after photosynthesis is shut down due to occlusion from sunlight [63]. Moreover, potential sources of error are the mismatch of diurnal cycles of both CO_2 and N_2O emissions and the one-time sampling of GHG emissions in practice. To reduce differences between observed and simulated fluxes, the timing of measurement was approximated to represent the average daily flux. However, this is difficult in practice and theory due to the inherent variability of the diurnal emissions cycles [64–66].

4.5. Intersection Sizes and Model Coherency

Indication for a possible N limitation of respiration can be found in the pair-wise partial intersections (see Table A5). The intersection between simulated biomass and CO_2 emissions (between P_{Biom} and P_{CO2}) showed by far the smallest partial pair-wise intersection size. Our interpretation is that a correct simulation of both biomass and CO_2 emissions is difficult within the current model setups. Reason for this may be that LandscapeDNDC forces the modelled ecosystem to increase both plant growth and respiration to approximate measured data of biomass and CO_2 emissions. If N limitation (as it was mentioned in Section 4.2) and the fixed C–N ratio leads to C limitation, the model tends to underestimate harvested biomass and/or CO_2 emissions as it is unable to allocate enough organic matter needed for growth and respiration. Simulating more aboveground biomass, for example, reduces exudation, root litter production and microbial biomass, all essential for soil respiration. This compromises model coherency since simulations tend to underestimate measurements in general and peak values (spring harvests for biomass and summer peaks for CO_2 emissions, see Figures 4

and 6) in particular. Such N limitation is more evident for the plot A1 where lowest NO_3^- uptake (Figure 3) coincides with lowest biomass and CO_2 emissions. Generally, this exemplifies an interesting characteristic of multi-variable calibration that choosing parameter sets (and thus, simulations) with emphasis to improve match with measurements for one target value is likely to impair match with (at least) one other target value [67–69]. For our revised model setup model withGW, this issue of N and C limitation remained even after groundwater implementation since the sizes of the intersections (both pair-wise and full) are similar for withGW and noGW simulations (see Section 3.1 and Table A5). This gives a different view than RMSE values only, that showed an improved match of biomass and CO_2 emissions with measured data for withGW simulations (see Tables 3 and 5). An analysis based solely on RMSE might mask functional feedback mechanisms between the C, N and water cycle.

Applications of multi-variable calibration ideally improve simulations of natural systems so that a more realistic representation of one system-relevant target value (like SWC) is prerequisite for improvement of another target value. However, this is rarely done, particularly not with intrinsically dependent target values such as GHG emissions, soil moisture and biomass. Houska et al. [70] achieved good results applying such an approach to a coupled plant growth—hydrological model to simulate SWC and different kinds of plant dry matter. Sitch et al. [71] achieved good results by simulating several ecosystem variables, including soil moisture and net ecosystem exchange, on local to global scales. However, we admit that such an analysis is challenging for target values that are highly dynamic in space and time. This applies in particular to trace gas emissions, where hot moments and hot spots are the rule rather than the exception.

5. Conclusions

LandscapeDNDC simulations of biomass and CO_2 emissions showed generally better agreement with measurements if groundwater-borne NO_3^- was represented in the calculations (withGW), wherefore we argue that lateral inflow of NO_3^--rich groundwater can have a considerable effect on the N cycle of the investigated grassland. The credibility of the N balance and biomass simulations benefitted most from the additional groundwater N source, while CO_2 and N_2O emissions showed less or no improvement as they are impaired by low quality SWC simulations. Model coherency (quantified by intersection sizes, see Table 2) has not improved in withGW simulations, perhaps indicating that the C cycle is still affected by N limitation or deficient soil moisture variability.

To this end, we advocate replacing watercycleDNDC with a more physically-based hydrological submodel. Kröbel et al. [58] applied watercycleDNDC to simulate the water dynamics of a floodplain, but argued for using the Richard's equation to calculate water movement and retention in periodically wet soils. This approach is used in the Catchment Modelling Framework (CMF, see [72]) that has already been used in combination with LandscapeDNDC for simulations on a virtual hillslope [21] resp. virtual landscape [22]. Application of the LandscapeDNDC-CMF model coupling to our study site is ongoing work. Furthermore, we conclude that more data on concentrations of NO_3^- and organic N in groundwater, preferably on daily resolution are needed. First measurements in six piezometers in close vicinity, which we also have used in this study showed a very high variability of NO_3^- concentrations in space and time, with a strong decline over the course of the year. Continuous, area-wide measurements over several years could provide the basis to approximate the seasonal cycle of the groundwater NO_3^- concentrations, thus delivering a more accurate picture of N supply.

Further improvements will be achieved by a thorough balancing of C, N and water cycles in accordance to the long-term measurements. This starts by including more recent field site data to extend the simulation period up to present time, allowing better insight into environmental long-term trends of soil C and N pools. Concerning the model setup, we recommend replacing grasslandDNDC with the recently published LandscapeDNDC physiology submodel [73] based on the Farquhar model for photosynthetic CO_2 assimilation [74], which has been tested so far for paddy rice systems. We assume that this will provide higher model sensitivity towards changing atmospheric CO_2 concentrations and allows for the simulations of grassland plots under CO_2 enrichment in the Giessen FACE experiment.

Author Contributions: Conceptualization, L.B. and P.K.; Data curation, R.L. and C.M.; Formal analysis, R.L.; Funding acquisition, L.B. and C.M.; Investigation, R.L.; Methodology, R.L., T.H., S.K., D.K. and E.H.; Project administration, L.B. and C.M.; Software, R.L., T.H., S.K., D.K. and E.H.; Supervision, L.B., C.M. and P.K.; Validation, R.L. and D.K.; Visualization, R.L.; Writing-original draft, R.L.; Writing-review & editing, R.L., L.B., T.H., S.K., D.K., E.H., C.M. and P.K.

Funding: This research was funded by the LOEWE excellence cluster FACE2FACE of the Hessen State Ministry of Higher Education, Research and the Arts.

Acknowledgments: The authors thank their colleagues for continuous support and discussion. Part of this work was funded by the LOEWE excellence cluster FACE2FACE of the Hessen State Ministry of Higher Education, Research and the Arts. We would like to further acknowledge the financial support provided by the Deutsche Forschungsgemeinschaft (DFG) for Tobias Houska (BR2238/13-1) and for Edwin Haas (BU1173/12-1). Edwin Haas received additional support by the FACCE-JPI MACSUR.

Conflicts of Interest: The authors declare no conflict of interest. The founding sponsors had no role in the design of the study; in the collection, analyses, or interpretation of data; in the writing of the manuscript, and in the decision to publish the results.

Appendix A

Table A1. Measured data implemented in LandscapeDNDC: FSM = field site measurements (see Section 2.1); WD = weather data [75]; variable = soil moisture, CO_2 and N_2O emissions measurements ranged from several per week to several per month.

Name	Value/Unit	Start/End	Temporal Resolution	Usage	Source
Air Temperature (Mean, Min, Max)	°C	1995/2009	daily	Driver data	WD
Global Radiation	W m^{-2}	1995/2009	daily	Driver data	WD
Precipitation	mm day^{-1}	1995/2009	daily	Driver data	WD
Relative Humidity	%	1995/2009	daily	Driver data	WD
Groundwater level	m	1995/2009	daily *1	Driver data	FSM
Cutting schedule	-	1995/2009	2/year	Driver data	FSM
Fertilizer application (ammonium nitrate)	40 kgN ha^{-1} $year^{-1}$	1995/2009	yearly	Driver data	[76]
N deposition	14 kgN ha^{-1} $year^{-1}$	1993/1995	mean	Driver data	[77]
Field capacity	mm m^{-1}	-	-	Calibrated parameter	[32]
Wilting point	mm m^{-1}	-	-	Calibrated parameter	[32]
Fraction of soil org. N	0.08–0.37%	2001/2002	-	Initialization	[31]
Fraction of soil org. C	0.69–3.96%	2001/2002	-	Initialization	[31]
Plant C/N ratio	25.7	1993/2009	average	Fixed parameter	FSM
Soil pH	5.4–6.0	-	-	Fixed parameter	[31]
Cutting height	4 cm	-	constant	Fixed parameter	FSM
Bulk density profile	1.01–1.52 g cm^{-3}	-	-	Fixed parameter	[32]
Texture (clay, silt, sand)	-	-	constant	Fixed parameter	[32]
CO_2 concentration	392.5 ppm	1998/2009	mean	Fixed parameter	FSM
Groundwater NO_3^- concentration	3.24 mg L^{-1}	2015	mean	Fixed parameter	FSM
CO_2 emissions	mg CO_2 m^{-2} h^{-1}	1998/2009	variable	Calibration data	FSM
N_2O emissions	µgN m^{-2} h^{-1}	1997/2009	variable monthly mean	Calibration data	FSM
Soil water content	%	1997/2009	variable *2	Calibration data	FSM
Biomass	kg ha^{-1} $year^{-1}$	1997/2009	2 cuts/year	Calibration data	FSM

*1 = groundwater levels have been recorded several times a week; missing values were linearly interpolated to provide daily data for model initialization; *2 = soil moisture data have been recorded several times per week, and removed of values that either (a) have been measured on days with air temperature below 0 °C, including the two subsequent days, or (b) exceeded the pore volume of the soil.

Table A2. Most sensitive LandscapeDNDC parameters. From left: internal LandscapeDNDC parameter name, parameters associated module, if the parameter was found sensitive for noGW/withGW, the lower and upper limits of the parameter range, process-related description.

Parameter Name	Module	Sensitive in Model Setup	Min	Max	Description
AMAXX	scDNDC	noGW, withGW	0.6545	1.9635	Microbial death rate
D_N2O	scDNDC	withGW	0.031	0.093	Reduction constant for N_2O diffusion
D_NO	scDNDC	withGW	0.0365	0.1095	Reduction constant for NO diffusion
DIFF_C	scDNDC	withGW	0.125	0.375	Diffusion constant for C compounds between aerobic and anaerobic microsites
DIFF_N	scDNDC	noGW, withGW	0.25	0.75	Diffusion constant for N compounds between aerobic and anaerobic microsites
DNDC_KMM_N_MIC	scDNDC	noGW	0.00058875	0.00294375	Michaelis-Menten constant for N dependency of microbial growth
EFF_NO2	scDNDC	noGW	0.214	0.642	Microbial efficiency for NO_2 denitrification
EFFAC	scDNDC	noGW, withGW	0.35	0.95	Fraction of decomposed C that goes to the dissolved organic C pool
FCO2_1	scDNDC	noGW	0.605	1.815	Factor for CO_2 production during humads decomposition process
FCO2_3	scDNDC	noGW	1.15	3.45	Like FCO2_1
FCO2_HU	scDNDC	noGW	0.4	1.2	Like FCO2_1
FNO3_U	scDNDC	noGW	0.375	0.9	Factor steering NO_3^- availability for microbial assimilation
KCHEM	scDNDC	noGW, withGW	4	12	Reaction rate for chemo-denitrification
KCRB_L	scDNDC	withGW	0.04625	0.13875	Decomposition constant for labile inactive microbes
KN2O	scDNDC	noGW, withGW	0.0025	0.0225	Reaction rate for N_2O reductase
KNIT	scDNDC	noGW, withGW	0.5	10	Reaction rate for nitrification
M_FACT_DEC1	scDNDC	noGW, withGW	0.2975	0.8925	Factor determining dependency of decomposition on water filled pore space
M_FACT_P1	scDNDC	noGW, withGW	0.225	0.675	Factor determining dependency of nitrification on water filled pore space
M_FACT_P6	scDNDC	noGW	5	15	Factor determining dependency of microbial activity on water filled pore space
MNO	scDNDC	noGW	0.0395	0.1185	Microbial maintenance coefficient for denitrification of NO
PERTVL	scDNDC	withGW	0.005	0.015	Downward transport of very labile litter
PHCRIT_N2O	scDNDC	noGW, withGW	2.5	7.5	Factor for pH dependency of N_2O denitrification
PHCRIT_NO2	scDNDC	noGW, withGW	3.05	9.15	Factor for pH dependency of NO_2 denitrification
TF_DEC1	scDNDC	noGW, withGW	1.77	5.31	Temperature dependency of decomposition
TF_NUP_N2O2	scDNDC	noGW, withGW	4.705	14.115	Temperature dependency of N_2O production during nitrification
sks_upper	wcDNDC	noGW, withGW	0.0007	0.7	Hydraulic conductivity of uppermost layer
wcmax_upper	wcDNDC	noGW, withGW	450	650	Field capacity of uppermost layer
wcmin_upper	wcDNDC	noGW, withGW	65	375	Wilting point of uppermost layer
ROOT	grDNDC	withGW	0.3	0.7	Root fraction of plant biomass

Table A3. Ranges of the statistical characteristics and measured data for noGW simulations during the investigation period. Mean, median and quantiles of the confidence intervals have been calculated for each time point of the period 1997–2009 (1998–2009 for CO_2 emissions). The depicted values show the ranges in which the statistics and measured data varied over time. Square brackets show the physical units of the target values.

Target Value	Plot	Simulations				Measurements
		Mean	Median	Quantile 2.5%	Quantile 97.5%	
N_2O emissions [$\mu gN\ m^{-2}\ h^{-1}$]	**A1**	0.72–25.31	0.46–21.19	0.03–6.15	2.80–68.32	0.36–99.04
	A2	0.80–24.35	0.56–21.30	0.13–9.12	2.21–54.15	−2.91–178.86
	A3	0.78–22.31	0.53–17.81	0.06–6.06	2.97–62.87	−1.00–104.81
CO_2 emissions [$mg\ m^{-2}\ h^{-1}$]	**A1**	8.51–408.84	2.68–407.55	0.42–311.26	43.94–546.79	27.6–1941.0
	A2	14.38–384.50	10.97–384.83	1.35–311.37	45.39–477.38	32.4–2409.0
	A3	12.38–389.74	5.51–388.12	0.55–295.32	49.07–547.58	18.4–2221.0
SWC [%]	**A1**	35.11–51.46	35.32–51.39	30.97–51.21	36.57–52.11	9.60–56.28
	A2	38.47–53.72	38.58–53.65	35.04–52.83	40.03–54.66	11.68–64.95
	A3	35.42–51.49	35.63–51.44	30.87–51.21	36.85–52.12	11.85–64.70
Biomass [$kg\ ha^{-1}$]	**A1**	1421–2281	1423–2308	1130–1874	1671–2714	1834–4833
	A2	1470–2341	1463–2348	1306–2100	1654–2614	2068–5630
	A3	1461–2301	1458–2329	1164–1951	1733–2871	1744–5511

Table A4. Ranges of the statistical characteristics and measured data for withGW simulations during the investigation period. Mean, median and quantiles of the confidence intervals have been calculated for each time point of the period 1997–2009 (1998–2009 for CO_2 emissions). The depicted values show the ranges in which the statistics and measured data varied over time. Round brackets show minimum values for the N deficit calculated from measurements, square brackets show the physical units of the target values.

Target Value	Plot	Simulations				Measurements
		Mean	Median	Quantile 2.5%	Quantile 97.5%	
N_2O emissions [$\mu gN\ m^{-2}\ h^{-1}$]	**A1**	0.69–27.84	0.45–22.56	0.03–5.80	2.36–82.87	0.36–99.04
	A2	0.89–57.04	0.53–50.52	0.07–9.81	3.31–169.52	−2.91–178.86
	A3	1.01–37.40	0.65–30.44	0.05–8.14	3.62–107.79	−1.00–104.81
CO_2 emissions [$mg\ m^{-2}\ h^{-1}$]	**A1**	9.4–474.7	3.4–460.0	0.5–319.7	51.3–708.7	27.6–1941.0
	A2	18.9–605.3	14.3–619.8	1.1 –325.7	56.7–952.6	32.4–2409.0
	A3	19.4–523.8	7.5–504.3	0.6–308.8	89.6–914.6	18.4–2221.0
SWC [%]	**A1**	35.36–51.45	35.51–51.39	30.97–51.20	36.92–52.00	9.60–56.28
	A2	30.28–53.63	30.58–53.61	24.97–52.88	34.52–54.64	11.68–64.95
	A3	37.02–51.49	37.13–51.47	33.60–51.20	38.39–52.24	11.85–64.70
Biomass [$kg\ ha^{-1}$]	**A1**	1828–3272	1836–3328	1280–2162	2248–4426	1834–4833
	A2	2499–4931	2468–5080	1561–2783	3154–6342	2068–5630
	A3	2323–4167	2356–4222	1418–2573	3070–5605	1744–5511
NO_3^- uptake [$kgN\ ha^{-1}$]	**A1**	3.89–54.41	4.15–57.78	0.33–4.49	6.73–93.97	(24.23–95.13)
	A2	44.95–121.31	56.54–130.57	3.21–6.78	71.53–193.88	(41.49–103.74)
	A3	32.26–81.44	33.32–84.14	3.11–6.40	56.98–142.36	(47.19–115.86)

Table A5. Pair-wise partial intersection sizes for withGW simulations: the number parameter sets that belong to the best 25% simulations of two target values.

Target Values	A1	A2	A3
Biomass—CO_2 emissions	8157	8252	8180
Biomass—N_2O emissions	52963	52948	53328
Biomass—Soil Moisture Content	34114	34324	34117
CO_2 emissions—N_2O emissions	23356	23146	23452
CO_2 emissions—Soil Moisture Content	38774	38710	38700
N_2O emissions—Soil Moisture Content	38582	38608	38561

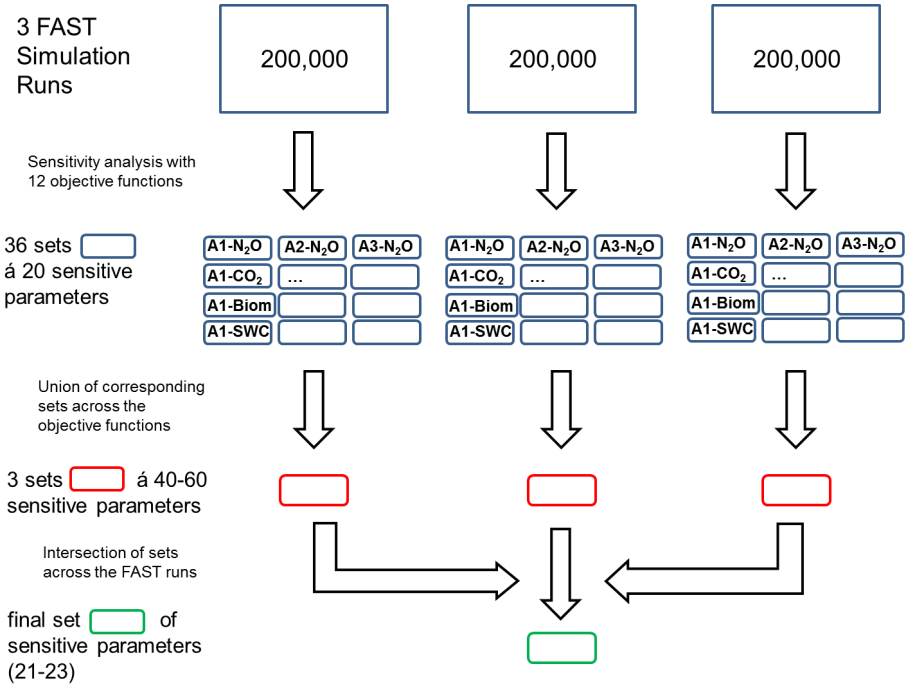

Figure A1. Sensitivity analysis diagram. For the calculation of the most sensitive parameters, 600,000 parameter sets have been sampled in 3 FAST runs. For each run, the 20 most sensitive parameters have been calculated separately for 12 objective functions (4 target values × 3 plots). After that, the sensitive parameters for each run have been unified. Finally, an intersection of the unified parameters was made among the FAST runs, creating the choice of sensitive parameters that was used for calibration.

References

1. Ciais, P.; Sabine, C.; Bala, G.; Bopp, L.; Brovkin, V.; Canadell, J.; Chhabra, A.; DeFries, R.; Galloway, J.; Heimann, M.; et al. Carbon and Other Biogeochemical Cycles. In *Climate Change 2013: The Physical Science Basis. Contribution of Working Group I to the Fifth Assessment Report of the Intergovernmental Panel on Climate Change*; Cambridge University Press: Cambridge, UK; New York, NY, USA, 2013.
2. Hartmann, D.L.; Klein Tank, A.M.G.; Rusticucci, M.; Alexander, L.V.; Brönnimann, S.; Charabi, Y.A.-R.; Dentener, F.J.; Dlugokencky, E.J.; Easterling, D.R.; Kaplan, A.; et al. Observations: Atmospheres and Surface. In *Climate Change 2013: The Physical Science Basis. Contribution of Working Group I to the Fifth Assessment Report of the Intergovernmental Panel on Climate Change*; Cambridge University Press: Cambridge, UK; New York, NY, USA, 2013.
3. Ravishankara, A.R.; Daniel, J.S.; Portmann, R.W. Nitrous Oxide (N_2O): The Dominant Ozone-Depleting Substance Emitted in the 21st Century. *Science* **2009**, *326*, 123–125. [CrossRef] [PubMed]

4. Syakila, A.; Kroeze, C. The global nitrous oxide budget revisited. *Greenh. Gas Meas. Manag.* **2011**, *1*, 17–26. [CrossRef]
5. Butterbach-Bahl, K.; Baggs, E.M.; Dannenmann, M.; Kiese, R.; Zechmeister-Boltenstern, S. Nitrous oxide emissions from soils: How well do we understand the processes and their controls? *Philos. Trans. R. Soc. B* **2013**, *368*, 20130122. [CrossRef] [PubMed]
6. Erisman, J.W.; Galloway, J.N.; Seitzinger, S.; Bleeker, A.; Dise, N.B.; Petrescu, A.M.R.; Leach, A.M.; de Vries, W. Consequences of human modification of the global nitrogen cycle. *Philos. Trans. R. Soc. B* **2013**, *368*, 20130116. [CrossRef] [PubMed]
7. Groffman, P.M.; Butterbach-Bahl, K.; Fulweiler, R.W.; Gold, A.J.; Morse, J.L.; Stander, E.K.; Tague, C.; Tonitto, C.; Vidon, P. Challenges to incorporating spatially and temporally explicit phenomena (hotspots and hot moments) in denitrification models. *Biogeochemistry* **2009**, *93*, 49–77. [CrossRef]
8. Christensen, S. Nitrous oxide emission from a soil under permanent grass: Seasonal and diurnal fluctuations as influenced by manuring and fertilization. *Soil Biol. Biochem.* **1983**, *15*, 531–536. [CrossRef]
9. Gleeson, D.B.; Müller, C.; Banerjee, S.; Ma, W.; Siciliano, S.D.; Murphy, D.V. Response of ammonia oxidizing archaea and bacteria to changing water filled pore space. *Soil Biol. Biochem.* **2010**, *42*, 1888–1891. [CrossRef]
10. Goodroad, L.L.; Keeney, D.R. Nitrous oxide production in aerobic soils under varying pH, temperature and water content. *Soil Biol. Biochem.* **1984**, *16*, 39–43. [CrossRef]
11. Shen, J.-P.; Xu, Z.; He, J.-Z. Frontiers in the microbial processes of ammonia oxidation in soils and sediments. *J. Soils Sediments* **2014**, *14*, 1023–1029. [CrossRef]
12. Smart, D.R.; Bloom, A.J. Wheat leaves emit nitrous oxide during nitrate assimilation. *Proc. Natl. Acad. Sci. USA* **2001**, *98*, 7875–7878. [CrossRef] [PubMed]
13. Smith, K.A.; Thomson, P.E.; Clayton, H.; Mctaggart, I.P.; Conen, F. Effects of temperature, water content and nitrogen fertilisation on emissions of nitrous oxide by soils. *Atmos. Environ.* **1998**, *32*, 3301–3309. [CrossRef]
14. Wrage, N.; Velthof, G.L.; van Beusichem, M.L.; Oenema, O. Role of nitrifier denitrification in the production of nitrous oxide. *Soil Biol. Biochem.* **2001**, *33*, 1723–1732. [CrossRef]
15. Müller, C.; Sherlock, R.R.; Williams, P.H. Mechanistic model for nitrous oxide emission via nitrification and denitrification. *Biol. Fertil. Soils* **1997**, *24*, 231–238. [CrossRef]
16. Ryan, M.; Müller, C.; Di, H.J.; Cameron, K.C. The use of artificial neural networks (ANNs) to simulate N_2O emissions from a temperate grassland ecosystem. *Ecol. Model.* **2004**, *175*, 189–194. [CrossRef]
17. Levy, P.E.; Mobbs, D.C.; Jones, S.K.; Milne, R.; Campbell, C.; Sutton, M.A. Simulation of fluxes of greenhouse gases from European grasslands using the DNDC model. *Agric. Ecosyst. Environ.* **2007**, *121*, 186–192. [CrossRef]
18. Xu, R.; Prentice, I.C.; Spahni, R.; Niu, H.S. Modelling terrestrial nitrous oxide emissions and implications for climate feedback. *New Phytol.* **2012**, *196*, 472–488. [CrossRef]
19. Tague, C.L.; Band, L.E. RHESSys: Regional Hydro-Ecologic Simulation System—An Object-Oriented Approach to Spatially Distributed Modeling of Carbon, Water, and Nutrient Cycling. *Earth Interact.* **2004**, *8*, 1–42. [CrossRef]
20. Cui, J.; Li, C.; Sun, G.; Trettin, C. Linkage of MIKE SHE to Wetland-DNDC for carbon budgeting and anaerobic biogeochemistry simulation. *Biogeochemistry* **2005**, *72*, 147–167. [CrossRef]
21. Kraft, P.; Haas, E.; Klatt, S.; Kiese, R.; Butterbach-Bahl, K.; Frede, H.-G.; Breuer, L. Modelling nitrogen transport and turnover at the hillslope scale—A process oriented approach. In *6th International Congress on Environmental Modelling and Software 2012*; International Environmental Modelling and Software Society (iEMSs): Leipzig, Germany, 2012; ISBN 978-88-9035-742-8.
22. Wlotzka, M.; Haas, E.; Kraft, P.; Heuveline, V.; Klatt, S.; Kraus, D.; Butterbach-Bahl, K.; Breuer, L. Dynamic Simulation of Land Management Effects on Soil N_2O Emissions using a coupled Hydrology-Ecosystem Model. *Prepr. Ser. Eng. Math. Comput. Lab.* **2013**. [CrossRef]
23. Klatt, S.; Kraus, D.; Kraft, P.; Breuer, L.; Wlotzka, M.; Heuveline, V.; Haas, E.; Kiese, R.; Butterbach-Bahl, K. Exploring impacts of vegetated buffer strips on nitrogen cycling using a spatially explicit hydro-biogeochemical modeling approach. *Environ. Model. Softw.* **2017**, *90*, 55–67. [CrossRef]
24. Brown, K.S.; Sethna, J.P. Statistical mechanical approaches to models with many poorly known parameters. *Phys. Rev. E* **2003**, *68*, 021904. [CrossRef] [PubMed]

25. Rahn, K.-H.; Werner, C.; Kiese, R.; Haas, E.; Butterbach-Bahl, K. Parameter-induced uncertainty quantification of soil N_2O, NO and CO_2 emission from Höglwald spruce forest (Germany) using the LandscapeDNDC model. *Biogeosciences* **2012**, *9*, 3983–3998. [CrossRef]
26. Confalonieri, R. Monte Carlo based sensitivity analysis of two crop simulators and considerations on model balance. *Eur. J. Agron.* **2010**, *33*, 89–93. [CrossRef]
27. Pappenberger, F.; Beven, K.J. Ignorance is bliss: Or seven reasons not to use uncertainty analysis. *Water Resour. Res.* **2006**, *42*, W05302. [CrossRef]
28. Beven, K.; Freer, J. Equifinality, data assimilation, and uncertainty estimation in mechanistic modelling of complex environmental systems using the GLUE methodology. *J. Hydrol.* **2001**, *249*, 11–29. [CrossRef]
29. Haas, E.; Klatt, S.; Fröhlich, A.; Kraft, P.; Werner, C.; Kiese, R.; Grote, R.; Breuer, L.; Butterbach-Bahl, K. LandscapeDNDC: A process model for simulation of biosphere–atmosphere–hydrosphere exchange processes at site and regional scale. *Landsc. Ecol.* **2013**, *28*, 615–636. [CrossRef]
30. Grünhage, L.; Schmitt, J.; Hertstein, U.; Janze, S.; Peter, M.; Jäger, H.-J., III. Beschreibung der Versuchsfläche. In *Auswirkungen dynamischer Veränderungen der Luftzusammensetzung und des Klimas auf terrestrische Ökosysteme in Hessen-II-Umweltbeobachtungs- und Klimafolgenforschungsstation Linden, Jahresbericht 1995*; Umweltplanung, Arbeits- und Umweltschutz: Wiesbaden, Germany, 1996; ISBN 3-89026-236-8.
31. Jäger, H.-J.; Schmidt, S.W.; Kammann, C.; Grünhage, L.; Müller, C.; Hanewald, K. The University of Giessen Free-Air Carbon dioxide Enrichment study: Description of the experimental site and of a new enrichment system. *J. Appl. Bot.* **2003**, *77*, 117–127.
32. Kammann, C.; Grünhage, L.; Jäger, H.-J., II. N_2O- und CH_4-Flüsse in der bodennahen Atmosphäre eines extensiv genutzten Grünlandökosystems. In *Auswirkungen dynamischer Veränderungen der Luftzusammensetzung und des Klimas auf terrestrische Ökosysteme in Hessen-III-Umweltbeobachtungs- und Klimafolgenforschungsstation Linden, Berichtszeitraum 1996–1999*; Umweltplanung, Arbeits- und Umweltschutz: Wiesbaden, Germany, 2000; ISBN 3-89026-311-9.
33. Näsholm, T.; Huss-Danell, K.; Högberg, P. Uptake of Organic Nitrogen in the Field by Four Agriculturally Important Plant Species. *Ecology* **2000**, *81*, 1155–1161. [CrossRef]
34. Grote, R.; Kiese, R.; Grünwald, T.; Ourcival, J.-M.; Granier, A. Modelling forest carbon balances considering tree mortality and removal. *Agric. For. Meteorol.* **2011**, *151*, 179–190. [CrossRef]
35. Stange, F.; Butterbach-Bahl, K.; Papen, H.; Zechmeister-Boltenstern, S.; Li, C.; Aber, J. A process-oriented model of N_2O and NO emissions from forest soils: 2. Sensitivity analysis and validation. *J. Geophys. Res. Atmos.* **2000**, *105*, 4385–4398. [CrossRef]
36. Werner, C.; Butterbach-Bahl, K.; Haas, E.; Hickler, T.; Kiese, R. A global inventory of N_2O emissions from tropical rainforest soils using a detailed biogeochemical model. *Glob. Biogeochem. Cycles* **2007**, *21*, GB3010. [CrossRef]
37. Saggar, S.; Giltrap, D.L.; Li, C.; Tate, K.R. Modelling nitrous oxide emissions from grazed grasslands in New Zealand. *Agric. Ecosyst. Environ.* **2007**, *119*, 205–216. [CrossRef]
38. Abdalla, M.; Kumar, S.; Jones, M.; Burke, J.; Williams, M. Testing DNDC model for simulating soil respiration and assessing the effects of climate change on the CO_2 gas flux from Irish agriculture. *Glob. Planet. Chang.* **2011**, *78*, 106–115. [CrossRef]
39. Molina-Herrera, S.; Haas, E.; Klatt, S.; Kraus, D.; Augustin, J.; Magliulo, V.; Tallec, T.; Ceschia, E.; Ammann, C.; Loubet, B.; et al. A modeling study on mitigation of N_2O emissions and NO_3 leaching at different agricultural sites across Europe using LandscapeDNDC. *Sci. Total Environ.* **2016**, *553*, 128–140. [CrossRef] [PubMed]
40. Li, C.; Frolking, S.; Frolking, T.A. A model of nitrous oxide evolution from soil driven by rainfall events: 1. Model structure and sensitivity. *J. Geophys. Res. Atmos.* **1992**, *97*, 9759–9776. [CrossRef]
41. Kiese, R.; Heinzeller, C.; Werner, C.; Wochele, S.; Grote, R.; Butterbach-Bahl, K. Quantification of nitrate leaching from German forest ecosystems by use of a process oriented biogeochemical model. *Environ. Pollut.* **2011**, *159*, 3204–3214. [CrossRef] [PubMed]
42. Grote, R.; Lavoir, A.-V.; Rambal, S.; Staudt, M.; Zimmer, I.; Schnitzler, J.-P. Modelling the drought impact on monoterpene fluxes from an evergreen Mediterranean forest canopy. *Oecologia* **2009**, *160*, 213–223. [CrossRef] [PubMed]
43. Houska, T.; Kraft, P.; Chamorro-Chavez, A.; Breuer, L. SPOTting Model Parameters Using a Ready-Made Python Package. *PLoS ONE* **2015**, *10*, e0145180. [CrossRef] [PubMed]

44. Cukier, R.I.; Fortuin, C.M.; Shuler, K.E.; Petschek, A.G.; Schaibly, J.H. Study of the sensitivity of coupled reaction systems to uncertainties in rate coefficients. I Theory. *J. Chem. Phys.* **1973**, *59*, 3873–3878. [CrossRef]
45. Saltelli, A.; Tarantola, S.; Chan, K.P.-S. A Quantitative Model-Independent Method for Global Sensitivity Analysis of Model Output. *Technometrics* **1999**, *41*, 39–56. [CrossRef]
46. McKay, M.D.; Beckman, R.J.; Conover, W.J. A Comparison of Three Methods for Selecting Values of Input Variables in the Analysis of Output from a Computer Code. *Technometrics* **1979**, *21*, 239–245. [CrossRef]
47. He, J.; Jones, J.W.; Graham, W.D.; Dukes, M.D. Influence of likelihood function choice for estimating crop model parameters using the generalized likelihood uncertainty estimation method. *Agric. Syst.* **2010**, *103*, 256–264. [CrossRef]
48. Pathak, T.B.; Jones, J.W.; Fraisse, C.W.; Wright, D.; Hoogenboom, G. Uncertainty Analysis and Parameter Estimation for the CSM-CROPGRO-Cotton Model. *Agron. J.* **2012**, *104*, 1363. [CrossRef]
49. Giese, M.; Brueck, H.; Gao, Y.Z.; Lin, S.; Steffens, M.; Koegel-Knabner, I.; Glindemann, T.; Susenbeth, A.; Taube, F.; Butterbach-Bahl, K.; et al. N balance and cycling of Inner Mongolia typical steppe: A comprehensive case study of grazing effects. *Ecol. Monogr.* **2013**, *83*, 195–219. [CrossRef]
50. Kreutzer, K.; Butterbach-Bahl, K.; Rennenberg, H.; Papen, H. The complete nitrogen cycle of an N-saturated spruce forest ecosystem. *Plant Biol.* **2009**, *11*, 643–649. [CrossRef] [PubMed]
51. Zhou, M.; Zhu, B.; Brüggemann, N.; Dannenmann, M.; Wang, Y.; Butterbach-Bahl, K. Sustaining crop productivity while reducing environmental nitrogen losses in the subtropical wheat-maize cropping systems: A comprehensive case study of nitrogen cycling and balance. *Agric. Ecosyst. Environ.* **2016**, *231*, 1–14. [CrossRef]
52. Paustian, K.; Andren, O.; Clarholm, M.; Hansson, A.-C.; Johansson, G.; Lagerlof, J.; Lindberg, T.; Pettersson, R.; Sohlenius, B. Carbon and Nitrogen Budgets of Four Agro-Ecosystems With Annual and Perennial Crops, With and Without N Fertilization. *J. Appl. Ecol.* **1990**, *27*, 60. [CrossRef]
53. Watson, C.J.; Jordan, C.; Kilpatrick, D.; McCarney, B.; Stewart, R. Impact of grazed grassland management on total N accumulation in soil receiving different levels of N inputs. *Soil Use Manag.* **2007**, *23*, 121–128. [CrossRef]
54. Müller, C.; Stevens, R.J.; Laughlin, R.J.; Jäger, H.-J. Microbial processes and the site of N_2O production in a temperate grassland soil. *Soil Biol. Biochem.* **2004**, *36*, 453–461. [CrossRef]
55. Regan, K.; Kammann, C.; Hartung, K.; Lenhart, K.; Müller, C.; Philippot, L.; Kandeler, E.; Marhan, S. Can differences in microbial abundances help explain enhanced N_2O emissions in a permanent grassland under elevated atmospheric CO_2? *Glob. Chang. Biol.* **2011**, *17*, 3176–3186. [CrossRef]
56. Luo, Q.; Gong, J.; Zhai, Z.; Pan, Y.; Liu, M.; Xu, S.; Wang, Y.; Yang, L.; Baoyin, T. The responses of soil respiration to nitrogen addition in a temperate grassland in northern China. *Sci. Total Environ.* **2016**, *569*, 1466–1477. [CrossRef] [PubMed]
57. Breuer, L.; Papen, H.; Butterbach-Bahl, K. N_2O emission from tropical forest soils of Australia. *J. Geophys. Res. Atmos.* **2000**, *105*, 26353–26367. [CrossRef]
58. Kröbel, R.; Sun, Q.; Ingwersen, J.; Chen, X.; Zhang, F.; Müller, T.; Römheld, V. Modelling water dynamics with DNDC and DAISY in a soil of the North China Plain: A comparative study. *Environ. Model. Softw.* **2010**, *25*, 583–601. [CrossRef]
59. Duretz, S.; Drouet, J.L.; Durand, P.; Hutchings, N.J.; Theobald, M.R.; Salmon-Monviola, J.; Dragosits, U.; Maury, O.; Sutton, M.A.; Cellier, P. NitroScape: A model to integrate nitrogen transfers and transformations in rural landscapes. *Environ. Pollut.* **2011**, *159*, 3162–3170. [CrossRef] [PubMed]
60. Xiang, S.-R.; Doyle, A.; Holden, P.A.; Schimel, J.P. Drying and rewetting effects on C and N mineralization and microbial activity in surface and subsurface California grassland soils. *Soil Biol. Biochem.* **2008**, *40*, 2281–2289. [CrossRef]
61. Sándor, R.; Barcza, Z.; Hidy, D.; Lellei-Kovács, E.; Ma, S.; Bellocchi, G. Modelling of grassland fluxes in Europe: Evaluation of two biogeochemical models. *Agric. Ecosyst. Environ.* **2016**, *215*, 1–19. [CrossRef]
62. Zhang, X.; Niu, G.-Y.; Elshall, A.S.; Ye, M.; Barron-Gafford, G.A.; Pavao-Zuckerman, M. Assessing five evolving microbial enzyme models against field measurements from a semiarid savannah—What are the mechanisms of soil respiration pulses? *Geophys. Res. Lett.* **2014**, *41*, 6428–6434. [CrossRef]
63. Amthor, J.S. The McCree–de Wit–Penning de Vries–Thornley Respiration Paradigms: 30 Years Later. *Ann. Bot.* **2000**, *86*, 1–20. [CrossRef]

64. Dong, Y.; Zhang, S.; Qi, Y.; Chen, Z.; Geng, Y. Fluxes of CO_2, N_2O and CH_4 from a typical temperate grassland in Inner Mongolia and its daily variation. *Chin. Sci. Bull.* **2000**, *45*, 1590–1594. [CrossRef]
65. Müller, C. Plants affect the in situ N_2O emissions of a temperate grassland ecosystem. Pflanzen beeinflussen die in situ N_2O-Freisetzungen eines Grünlandökosystems in temperierten Breiten. *J. Plant Nutr. Soil Sci.* **2003**, *166*, 771–773. [CrossRef]
66. Šimek, M.; Hynšt, J.; Šimek, P. Emissions of CH_4, CO_2, and N_2O from soil at a cattle overwintering area as affected by available C and N. *Appl. Soil Ecol.* **2014**, *75*, 52–62. [CrossRef]
67. Klepper, O. Multivariate aspects of model uncertainty analysis: Tools for sensitivity analysis and calibration. *Ecol. Model.* **1997**, *101*, 1–13. [CrossRef]
68. Wutzler, T.; Carvalhais, N. Balancing multiple constraints in model-data integration: Weights and the parameter block approach. *J. Geophys. Res. Biogeosci.* **2014**, *119*, 2112–2129. [CrossRef]
69. Yapo, P.O.; Gupta, H.V.; Sorooshian, S. Multi-objective global optimization for hydrologic models. *J. Hydrol.* **1998**, *204*, 83–97. [CrossRef]
70. Houska, T.; Multsch, S.; Kraft, P.; Frede, H.-G.; Breuer, L. Monte Carlo-based calibration and uncertainty analysis of a coupled plant growth and hydrological model. *Biogeosciences* **2014**, *11*, 2069–2082. [CrossRef]
71. Sitch, S.; Smith, B.; Prentice, I.C.; Arneth, A.; Bondeau, A.; Cramer, W.; Kaplan, J.O.; Levis, S.; Lucht, W.; Sykes, M.T.; et al. Evaluation of ecosystem dynamics, plant geography and terrestrial carbon cycling in the LPJ dynamic global vegetation model. *Glob. Chang. Biol.* **2003**, *9*, 161–185. [CrossRef]
72. Kraft, P.; Vaché, K.B.; Frede, H.-G.; Breuer, L. CMF: A Hydrological Programming Language Extension For Integrated Catchment Models. *Environ. Model. Softw.* **2011**, *26*, 828–830. [CrossRef]
73. Kraus, D.; Weller, S.; Klatt, S.; Haas, E.; Wassmann, R.; Kiese, R.; Butterbach-Bahl, K. A new LandscapeDNDC biogeochemical module to predict CH_4 and N_2O emissions from lowland rice and upland cropping systems. *Plant Soil* **2014**, *386*, 125–149. [CrossRef]
74. Farquhar, G.D.; von Caemmerer, S.; Berry, J.A. A biochemical model of photosynthetic CO_2 assimilation in leaves of C3 species. *Planta* **1980**, *149*, 78–90. [CrossRef] [PubMed]
75. Dämmgen, U.; Grünhage, L.; Schaaf, S. The precision and spatial variability of some meteorological parameters needed to determine vertical fluxes of air constituents. *Landbauforsch. Volkenrode* **2005**, *55*, 29–37.
76. Kammann, C.; Müller, C.; Grünhage, L.; Jäger, H.-J. Elevated CO_2 stimulates N_2O emissions in permanent grassland. *Soil Biol. Biochem.* **2008**, *40*, 2194–2205. [CrossRef]
77. Scholz-Seidel, C. Dämmgen, U.V.2 Messungen der Bulk-Depositionen sedimentierender anorganischer Spezies (September 1993 bis Dezember 1995). In *Auswirkungen dynamischer Veränderungen der Luftzusammensetzung und des Klimas auf terrestrische Ökosysteme in Hessen-II-Umweltbeobachtungs- und Klimafolgenforschungsstation Linden, Jahresbericht 1995*; Umweltplanung, Arbeits- und Umweltschutz: Wiesbaden, Germany, 1996; ISBN 3-89026-236-8.